ELSEVIER

www.elsevier.nl/locate/jorganchem

Journal of Organometallic Chemistry 596 (2000) 36–45

Journal of Organometallic Chemistry

Synthesis, characterization and crystal structures of some tungsten and triosmium carbonyl complexes with monopyridyl and dipyridyl azo ligands

Wai-Yeung Wong [a,*], Suk-Ha Cheung [a], Siu-Ming Lee [a], Sze-Yin Leung [b]

[a] *Department of Chemistry, Hong Kong Baptist University, Waterloo Road, Kowloon Tong, Hong Kong, People's Republic of China*
[b] *Department of Chemistry, The University of Hong Kong, Pokfulam Road, Hong Kong, People's Republic of China*

Received 6 July 1999

Dedicated to Professor F.A. Cotton on the occasion of his 70th birthday.

Abstract

Substitution reactions of $[W(CO)_5(THF)]$ with the azo-functionalized monopyridyl and dipyridyl ligands, namely, 4-phenylazopyridine $\mathbf{L_1}$ and 4,4′-azopyridine $\mathbf{L_2}$, readily afford two tungsten carbonyl complexes $[W(CO)_5(NC_5H_4–N=N–C_6H_5)]$ (**1**) and $[(CO)_5W(\mu\text{-}NC_5H_4–N=N–C_5H_4N)W(CO)_5]$ (**2**) in good yields. Ligation of $\mathbf{L_1}$ and $\mathbf{L_2}$ with the activated triosmium carbonyl cluster $[Os_3(CO)_{10}(NCMe)_2]$ by *ortho*-metallation reaction provides $[Os_3(\mu\text{-}H)(CO)_{10}(\mu\text{-}NC_5H_3–N=N–C_6H_5)]$ (**3**) and the linking cluster $[Os_3(\mu\text{-}H)(CO)_{10}(\mu\text{-}NC_5H_3–N=N–C_5H_3N)Os_3(\mu\text{-}H)(CO)_{10}]$ (**4**) in satisfactory yields. All of the complexes have been fully characterized by IR, ^{1}H-NMR, UV–vis spectroscopies, fast atom bombardment (FAB) mass spectrometry and electrochemical measurements. The solid-state molecular structures of **1**–**4** have been ascertained by single-crystal X-ray diffraction methods. The structures of **1** and **3** involve the coordination of $\mathbf{L_1}$ to one $\{W(CO)_5\}$ and $\{Os_3(CO)_{10}\}$ moieties, respectively. In the case of **2** and **4**, two identical metal cores are linked together by the bridging ligand $\mathbf{L_2}$. Spectroscopic investigations revealed that the metal-to-ligand charge transfer (MLCT) transitions of **1** and **2** demonstrate strong solvent dependency, displaying a large negative solvatochromism in a wide range of organic solvents. © 2000 Elsevier Science S.A. All rights reserved.

Keywords: Osmium; Tungsten; Clusters; Crystal structure; Solvatochromism

1. Introduction

Pyridines and their derivatives have been shown to be good monodentate ligands in coordination and cluster chemistry [1]. With suitable molecular design, two or more metal centers could be held in the same molecule for the investigation of metal–metal interactions [2]. In fact, dipyridyl bridging ligands incorporating the alkyne functionality have been widely used for the construction of dinuclear complexes [3], where the strong metal-to-ligand charge transfer (MLCT) normally present in metal pyridyl complexes is believed to be important for the design of nonlinear optical materials [4,5]. However, the coordination properties of closely related dipyridyl ligands comprising the azo (–N=N–) functional moiety, namely 4,4′-azopyridine $\mathbf{L_2}$, have received less attention [6]. Recent studies have demonstrated that the complexes $[\{Re(CO)_3(N–N)\}_2(\mathbf{L_2})][ClO_4]_2$ (N–N = 2,2′-bipyridine, 1,10-phenanthroline) exhibit intriguing photophysical properties [7].

On the other hand, the chemistry of carbonyl clusters of the iron triad containing azo ligands has been extensively investigated [8]. Wong and coworkers recently isolated two triosmium carbonyl clusters $[Os_3(CO)_{10}(\mu\text{-}\eta^3\text{-}NC_5H_4–N=N–Ph)]$ and $[Os_3(\mu\text{-}H)(CO)_{10}(\mu\text{-}\eta^2\text{-}NC_5H_3–N=N(O)–Ph)]$ from the reaction of $[Os_3(CO)_{10}(NCMe)_2]$ with the unsymmetrical 2-phenylazopyridine at room temperature (Scheme 1), indicating the preference of azo coordination to the triosmium framework over the alternative *ortho*-metallation of the α-C–H bond [9]. Taking into account the fact that the symmetrical 4,4′-azopyridine ligand could serve as a

* Corresponding author. Fax: +852-23397348.
E-mail address: rwywong@net1.hkbu.edu.hk (W.-Y. Wong)

0022-328X/00/$ - see front matter © 2000 Elsevier Science S.A. All rights reserved.
PII: S0022-328X(99)00536-7

versatile bridging ligand and has the potential to act as a linking group between cluster units, we decided to undertake a series of reactions between osmium carbonyl complexes and $\mathbf{L_2}$ in the expectation of forming polynuclear species that are relatively inert kinetically, which might be of interest as intermediates in the synthesis of high-nuclearity carbonyl clusters. In this report, we present the results of such a study. We also describe the synthesis of a dinuclear tungsten carbonyl complex bridged by $\mathbf{L_2}$ and some related carbonyl compounds bearing the monopyridyl-azo ligand, 4-phenylazopyridine $\mathbf{L_1}$.

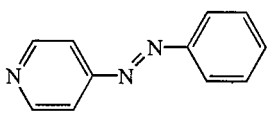

$\mathbf{L_1}$

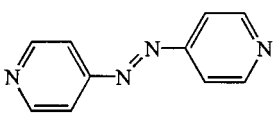

$\mathbf{L_2}$

2. Results and discussion

2.1. Synthesis

The syntheses of all new compounds are outlined in Scheme 2. The facile displacement of one carbonyl ligand of $W(CO)_6$ by pyridines [3,10] to give $(CO)_5(NC_5H_4R)]$ was successfully applied to the preparation of $[W(CO)_5(NC_5H_4–N{=}N–C_6H_5)]$ (**1**) and $[(CO)_5W(\mu\text{-}NC_5H_4–N{=}N–C_5H_4N)W(CO)_5]$ (**2**). Monosubstituted tungsten carbonyl complex **1** was readily prepared by reacting one equivalent of 4-phenylazopyridine $\mathbf{L_1}$ with $[W(CO)_5(THF)]$ prepared in situ from photolysis of $W(CO)_6$ in THF. Treatment of two molar equivalents of $[W(CO)_5(THF)]$ with $\mathbf{L_2}$ afforded a symmetrically bridged dimer **2**. Workup by column chromatography on silica is necessary to isolate these complexes in high purity and they are obtained as red (**1**) and deep-purple (**2**) solids in 47 and 53% yields, respectively. The metal clusters $[Os_3(\mu\text{-}H)(CO)_{10}(\mu\text{-}NC_5H_3–N{=}N–C_6H_5)]$ (**3**) and $[Os_3(\mu\text{-}H)(CO)_{10}(\mu\text{-}NC_5H_3–N{=}N–C_5H_3N)Os_3(\mu\text{-}H)(CO)_{10}]$ (**4**) are oxidative-addition products of the reaction of $[Os_3(CO)_{10}(NCMe)_2]$ with $\mathbf{L_1}$ and $\mathbf{L_2}$, respectively. The formation of both poses no conceptual problems. They are the results of *ortho*-metallation of the pyridyl ring in the ligands accompanied by C–H bond cleavage α to the nitrogen donor site and loss of MeCN groups. Subsequent purification by preparative thin-layer chromatography (TLC) on silica led to the isolation of **3** and **4** as orange and deep-red solids in fairly good yields. All the compounds in this study are found to be air-stable and soluble in common organic solvents.

2.2. Solution spectroscopy

The molecular formulae of all the new complexes were initially established by fast atom bombardment (FAB) MS, IR and ^{1}H-NMR spectroscopies. The spectroscopic properties are in accordance with their formulation and the data are summarized in Table 1. The three medium/strong carbonyl stretching ν_{CO} absorptions for **1** and **2** in the IR spectra are typical of a C_{4v} arrangement of CO groups at the metal center [3,10b]. For clusters **3** and **4**, their IR carbonyl spectra in CH_2Cl_2 have a similar ν_{CO} band pattern in the region 2200–1600 cm^{-1} and are reminiscent of the μ-pyridyl clusters $[Os_3(\mu\text{-}H)(CO)_{10}(\mu\text{-}NC_5H_3R)]$ (R = H, alkyl, anthryl, ferrocenyl derivatives, etc.) [11] and of other related *ortho*-metallated nitrogen-heterocyclic compounds [12]. This suggests the N,C-mode of attachment to the osmium atoms and the azo moiety remains intact

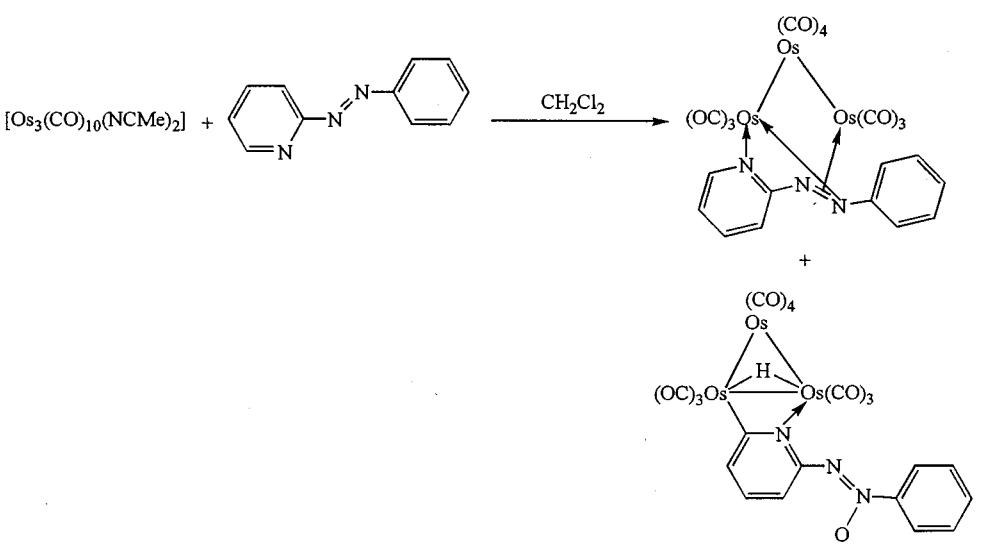

Scheme 1.

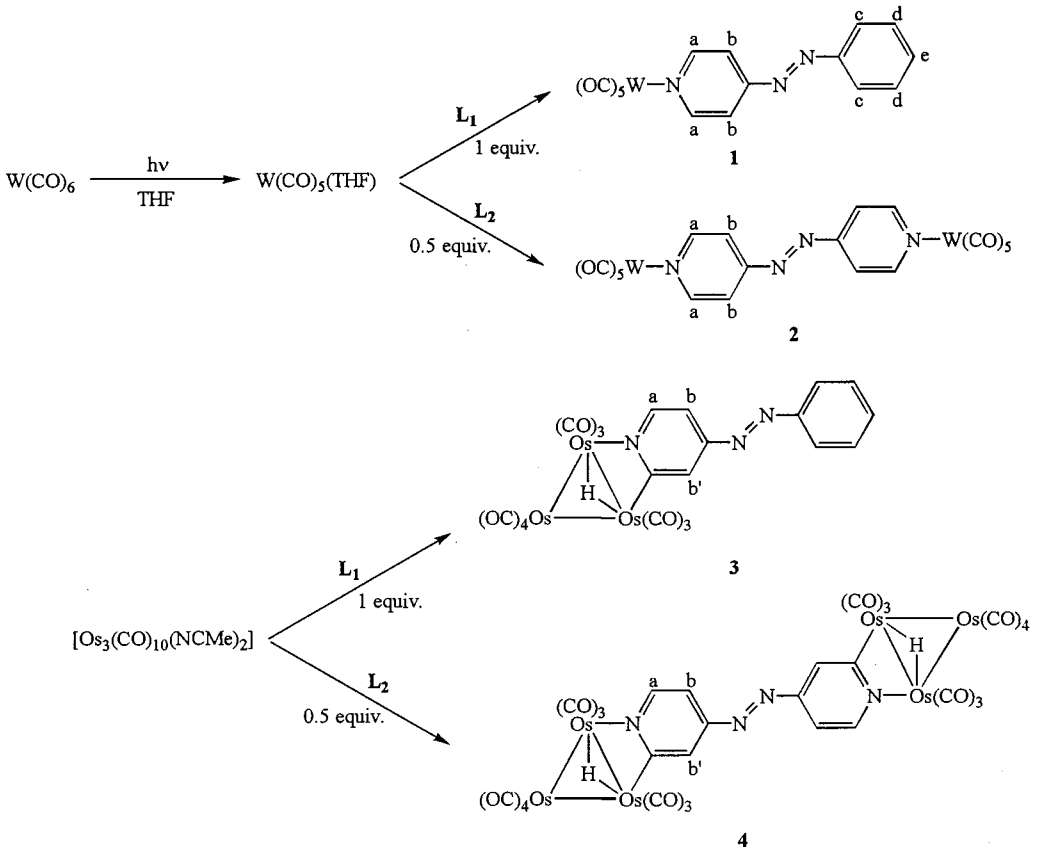

Scheme 2.

Table 1
Spectroscopic data for complexes **1**–**4**

Complex	IR (ν_{CO}) (cm^{-1}) [a]	^{1}H-NMR (δ, J in Hz) [b]	FAB MS (m/z) [c]
1	2072m, 1975sh, 1929s, 1896m	8.99 (dd, 2H, $J = 5.3$, 1.6, H_a), 7.99 (dd, 2H, $J = 6.8$, 1.9, H_c), 7.67 (dd, 2H, $J = 5.3$, 1.6, H_b), 7.59 (m, 3H, H_d, H_e)	507 (507)
2	2070m, 1978w, 1932s, 1900m	9.11 (d, 4H, $J = 6.8$, H_a), 7.73 (d, 4H, $J = 6.8$, H_b)	832 (832)
3	2104w, 2063vs, 2053vs, 2019vs, 2008vs, 1990s	8.26 (d, 1H, $J = 6.1$, H_a), 7.94 (m, 2H, C_6H_5), 7.74 (d, 1H, $J = 1.8$, $H_{b'}$), 7.53 (m, 3H, C_6H_5), 7.07 (dd, 1H, $J = 6.1$, 1.8, H_b), −14.74 (s, 1H, OsH)	1034 (1034)
4	2104m, 2063vs, 2054vs, 2020s, 2008s, 1992sh	8.31 (d, 2H, $J = 6.1$, H_a), 7.73 (d, 2H, $J = 1.8$, $H_{b'}$), 7.07 (dd, 2H, $J = 6.1$, 1.8, H_b), −14.71 (s, 2H, OsH)	1885 (1885)

[a] CH_2Cl_2.
[b] $CDCl_3$.
[c] Simulated masses in parentheses.

without being coordinated to the cluster framework. The compounds all display molecular ion envelopes of high to medium intensity in their positive FAB mass spectra, conforming to the stoichiometry of each complex.

The ^{1}H-NMR spectra of all the complexes show resonances due to the protons associated with the ligands, and in the case of **3** and **4**, the bridging hydrides on the Os–Os edges. For **1** and **2**, the pyridine ring *ortho*-protons experience a downfield shift in the chemical shift values upon coordination as compared with the free ligands, and the NC_5H_4 rings are essentially analyzed as AA′BB′ spin systems. The ^{1}H-NMR spectra of **3** and **4** in $CDCl_3$ further confirm *ortho*-metallation of the heterocycle. The three pyridyl protons H_a, H_b and $H_{b'}$ are mutually coupled with each other to give two doublets and a double doublet. The most downfield signal is ascribed to the *ortho*-proton which integrates as one proton against the hydride resonance.

2.3. Electronic absorption spectroscopy

Table 2 presents the electronic spectral data for the new complexes **1**–**4** in CH_2Cl_2 at room temperature along with those corresponding to the free ligands $\mathbf{L_1}$ and $\mathbf{L_2}$. In view of the characteristic solvent dependency of the absorption bands of tungsten pyridyl complexes [3], the electronic spectra of **1** and **2**, in a variety of organic solvents with different polarities, have also been measured. The UV–vis spectra of both $\mathbf{L_1}$ and $\mathbf{L_2}$ essentially consist of $\pi \rightarrow \pi^*$ transitions in the range 286–312 nm and $n \rightarrow \pi^*$ bands at 449 ($\mathbf{L_1}$) and 459 nm ($\mathbf{L_2}$) [6]. Apart from the intense bands in the near UV region due to the ligand-localized transitions, the $\{W(CO)_5(py)\}$-type chromophores of **1** and **2** also undergo a typical d–d transition near 400 nm which is relatively invariant [13]. It is interesting to note that both **1** and **2** exhibit a $W \rightarrow L(\pi^*)$ MLCT transition in the visible region beyond 400 nm which is strongly solvent dependent [3,13]. These absorption bands display significant negative solvatochromism in organic solvents of varying polarities (Table 2). The red shift of 56 nm for **1** and 120 nm for **2** in absorption energies from acetone to hexane in order of decreasing polarity is consistent with the charge-transfer nature of the transition [14].

The absorption spectra of **3** and **4** are dominated by the intense bands in the UV region that arise from the metal-perturbed intraligand $\pi \rightarrow \pi^*$ transitions. In the visible region an additional broad absorption shoulder is observed beyond 420 nm in each case, which is most likely to be cluster-centered. It is noteworthy that there is no evidence of solvatochromic shift for **3** and **4**.

2.4. Electrochemistry

The electrochemical properties of the monomeric and dimeric complexes **1**–**4** as well as their ligand precursors $\mathbf{L_1}$ and $\mathbf{L_2}$ were investigated in deoxygenated CH_2Cl_2 by cyclic voltammetry using $[NBu_4]PF_6$ as the supporting electrolyte. Redox potential values obtained in this study are given in Table 3. Both ligands $\mathbf{L_1}$ and $\mathbf{L_2}$ undergo two reduction processes in the potential range -1.30 to -2.09 V, which are either quasi-reversible or irreversible. For **1**–**4**, two ligand-centered reduction events were also apparent within the limits of the solvent window, analogous to complexes such as $[\{W(CO)_5\}_2(\mu\text{-}4,4'\text{-bipyridine})]$ [3,15a]. Based on these electrochemical data, it seems that there is no electronic communication between metal centers in the dimeric complexes even through such a fully conjugated ligand system [15b]. However, we observe a different degree of potential shifts for the ligand-localized reduction processes in **1** and **2**. Although there is almost no shift in reduction potentials for the tungsten mono complex **1** as compared with $\mathbf{L_1}$, a significant shift to less negative reduction potentials was observed in **2** upon complex formation with respect to $\mathbf{L_2}$, suggesting that the communication between the ligand and the metal center is better in the dimer **2**. Similar to other tungsten carbonyl complexes having pyridyl ligands, the $\{W(CO)_5(NC_5H_4)\}$ unit in **1** and **2** is redox active and both **1** and **2** display a chemically irreversible tungsten-centered oxidation at ca. 0.09 and 0.04 V, respectively (vs. Fc/Fc^+).

Table 2
UV–vis spectral data (nm) for complexes **1**–**4** [a]

Compound	C_6H_{14}	$CHCl_3$	CH_2Cl_2	MeOH	$(CH_3)_2CO$
1	486 (0.9)	447 (0.7)	441 (0.7)	437 (0.8)	430 (0.8)
	404 (0.6)	404 (0.7)	403 (0.7)	403 (0.9)	400 (0.9)
	321 (2.1)	321 (1.9)	321 (1.8)	289 (3.4)	331 (1.7)
	242 (7.5)	242 (8.0)	243 (6.3)	237 (1.5)	
2	610 (1.6)	565 (1.2)	535 (1.5)	498 (0.9)	490 (0.8)
	400 (0.7)	397 (0.8)	400 (1.0)	400 (0.9)	398 (0.8)
	243 (14.5)	242 (17.9)	244 (15.5)	269 (35.9)	
3			420sh (0.2)		
			325 (1.3)		
			289 (2.0)		
4			468sh (0.3)		
			373 (0.9)		
			324 (1.4)		
$\mathbf{L_1}$			449 (0.09)		
			312 (2.2)		
$\mathbf{L_2}$			459 (0.06)		
			286 (2.7)		

[a] Extinction coefficients ($\varepsilon \times 10^{-4}$) are shown in parentheses.

Table 3
Electrochemical data for complexes **1**–**4** in CH_2Cl_2 [a]

Compound	$E_{1/2}$ (red)	$E_{1/2}$ (ox)
$\mathbf{L_1}$	−1.30 [b], −1.78[b]	
$\mathbf{L_2}$	−1.61 [b], −2.09 [c]	
1	−1.32 [b], −1.78 [c]	0.09 [c]
2	−0.93 [b], −1.37 [c]	0.04 [c]
3	−1.47 [c], −1.88 [c]	
4	−1.13 [c], −2.38 [c]	

[a] The electrochemical measurements were made at a glassy carbon working electrode containing 0.1 M $[NBu_4]PF_6$ as base electrolyte, using a scan rate of 100 mV s^{-1}. All potentials were quoted in volts vs. the ferrocene/ferrocenium couple that was used as an internal standard.

[b] Quasi-reversible wave.

[c] Irreversible wave.

2.5. Crystal structure analyses

In order to substantiate the proposed structures of the newly synthesized compounds, single-crystal X-ray analyses were carried out for **1**–**4**. Red crystals of **1** and **4**, purple crystals of **2** and orange crystals of **3** suitable for diffraction studies were grown by slow evaporation of their respective solutions in an *n*-hexane–CH_2Cl_2 solvent mixture at room temperature. Perspective drawings of the molecular structures of **1**–**4** are depicted in Figs. 1–4, respectively, which include the atom-numbering scheme. Pertinent interatomic distances and angles are listed in Tables 4–8. For **1** and **2**, each tungsten atom has an approximately octahedral geometry and the W–C–O bonds do not show significant deviations from linearity (176(1)–177(1)° for **1**, 175(2)–178(2)° for **2**). The average C≡O bond lengths for **1** and **2** are 1.13(1) and 1.13(3) Å, respectively. The crystal structure of **2** comprises discrete dimeric molecules in which two halves of the molecule are related by a center of symmetry at the mid-point of the N(2)–N(2*) bond. The W–N(pyridyl) distance is 2.27(1) Å in each case, which is comparable to literature values [15]. By virtue of the apparent *trans* effect, the W–C bonds *trans* to the pyridyl ligands (W(1)–C(3) = 1.99(1) Å for **1**, 1.98(2) Å for **2**) are significantly shorter than other W–C bonds (2.03(3)–2.09(2) Å). The orientation of the coordinated pyridyl ring with respect to the tungsten fragment is defined by the angle between the pyridyl plane and the best plane consisting of the W, N and three CO ligands. In this way, the pyridyl ring is at an angle of 18.4 (**1**) and 21.6° (**2**) to the W(1)–N(1)–C(1)–C(3)–C(4) mean plane. The aromatic rings (py, Ph) in **1** and **2** are essentially coplanar and the largest deviations of atoms

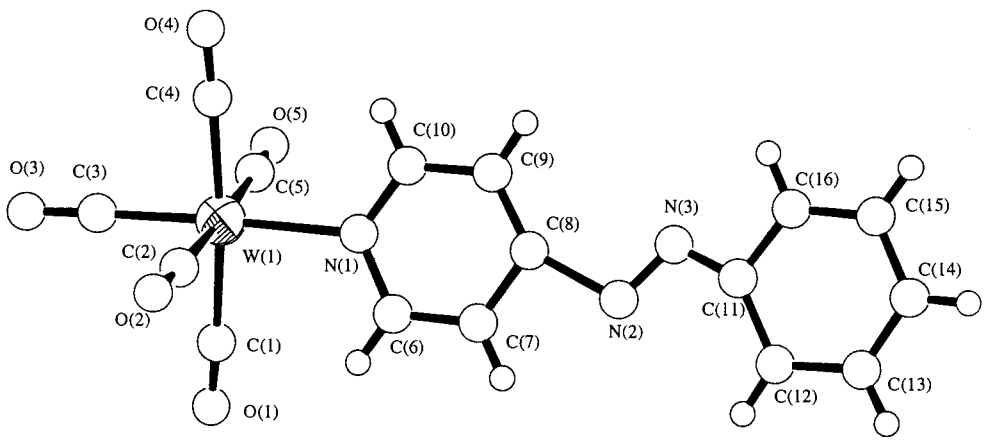

Fig. 1. Molecular structure of **1**, showing the atomic labeling scheme.

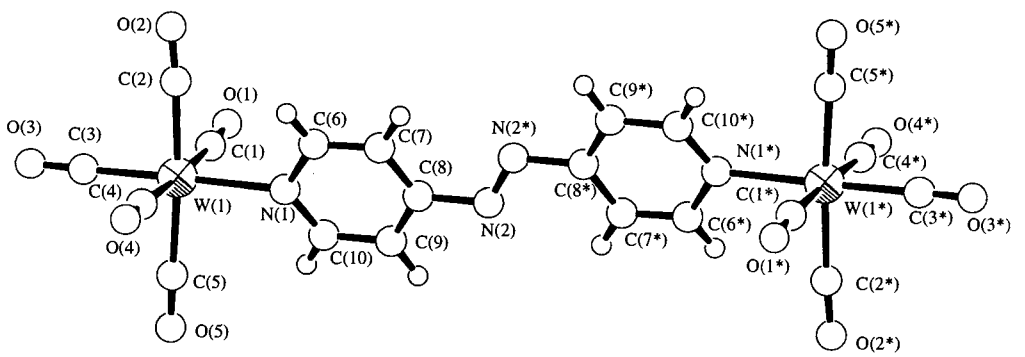

Fig. 2. Molecular structure of **2**, showing the atomic labeling scheme.

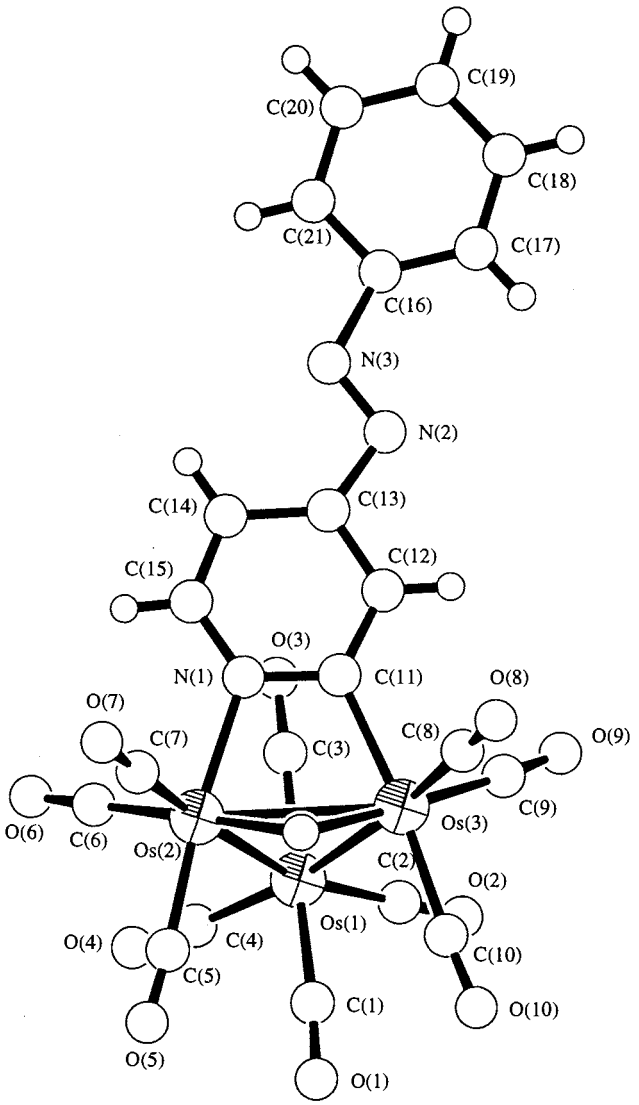

Fig. 3. Molecular structure of **3**, showing the atomic labeling scheme.

Table 4
Selected bond lengths (Å) and angles (°) for complex **1**

Bond lengths			
W(1)–C(1)	2.05(1)	W(1)–C(2)	2.06(1)
W(1)–C(3)	1.99(1)	W(1)–C(4)	2.06(1)
W(1)–C(5)	2.06(1)	W(1)–N(1)	2.270(8)
C(8)–N(2)	1.65(2)	N(2)–N(3)	1.23
N(3)–C(11)	1.26(1)		
Bond angles			
C(1)–W(1)–N(1)	92.6(4)	C(2)–W(1)–N(1)	91.1(4)
C(3)–W(1)–N(1)	177.7(5)	C(4)–W(1)–N(1)	93.2(4)
C(5)–W(1)–N(1)	92.3(4)	C(1)–W(1)–C(2)	89.1(5)
C(1)–W(1)–C(3)	85.9(5)	C(1)–W(1)–C(4)	174.1(4)
C(1)–W(1)–C(5)	90.5(5)	C(2)–W(1)–C(3)	87.1(5)
C(2)–W(1)–C(4)	91.6(5)	C(2)–W(1)–C(5)	176.6(4)
C(3)–W(1)–C(4)	88.4(5)	C(3)–W(1)–C(5)	89.5(5)
C(4)–W(1)–C(5)	88.4(5)	C(8)–N(2)–N(3)	106.5(7)
N(2)–N(3)–C(11)	109(1)		

Table 5
Selected bond lengths (Å) and angles (°) for complex **2**

Bond lengths			
W(1)–C(1)	2.03(3)	W(1)–C(2)	2.03(3)
W(1)–C(3)	1.98(2)	W(1)–C(4)	2.09(2)
W(1)–C(5)	2.08(4)	W(1)–N(1)	2.27(1)
C(8)–N(2)	1.47(2)	N(2)–N(2*)	1.14(3)
Bond angles			
C(1)–W(1)–N(1)	87.2(7)	C(2)–W(1)–N(1)	92.7(8)
C(3)–W(1)–N(1)	178.0(9)	C(4)–W(1)–N(1)	93.3(7)
C(5)–W(1)–N(1)	92.0(7)	C(1)–W(1)–C(2)	87(1)
C(1)–W(1)–C(3)	91.5(9)	C(1)–W(1)–C(4)	176.3(9)
C(1)–W(1)–C(5)	90(1)	C(2)–W(1)–C(3)	88(1)
C(2)–W(1)–C(4)	88(1)	C(2)–W(1)–C(5)	174.9(9)
C(3)–W(1)–C(4)	88(1)	C(3)–W(1)–C(5)	86(1)
C(4)–W(1)–C(5)	93.0(9)	C(8)–N(2)–N(2*)	116(2)

from the least-squares planes are, respectively, 0.005 and 0.01 Å for the py and Ph rings in **1** and 0.02 Å for the py ring in **2**. The dihedral angle between the py and

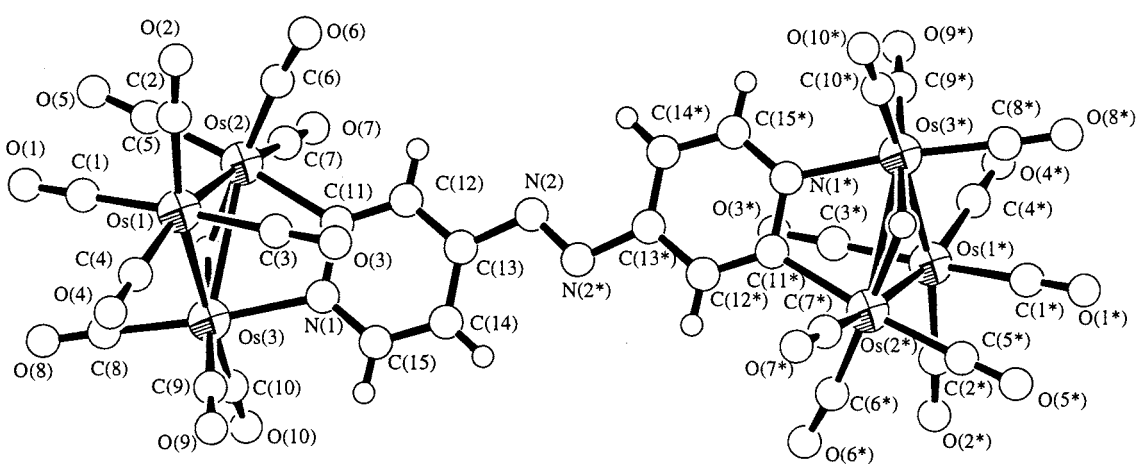

Fig. 4. Molecular structure of **4**, showing the atomic labeling scheme.

Ph mean planes is 2.43° in **1**. All the aromatic bond lengths and angles are within the expected ranges.

The structures of both **3** and **4** reveal an *ortho*-metallation of the pyridyl ring, arising from C–H fission and transfer of an *ortho*-hydrogen atom to the osmium atoms. This is consistent with the structural assignment from spectroscopic studies. It is obvious from Fig. 4 that the structure of **4** contains two triosmium units linked by a 4,4′-azopyridine bridging moiety and both ends of the pyridyl groups of $\mathbf{L_2}$ have undergone *ortho*-metallation. In the crystal lattice, the molecule of **4** is symmetrical with a crystallographic C_i symmetry passing through the central point of the N=N bond. The essential features of both structures are quite similar. Within the osmium triangle in each case, there are altogether ten terminal carbonyl ligands, four to Os(1) and three each to Os(2) and Os(3). The pyridyl rings of $\mathbf{L_1}$ and $\mathbf{L_2}$ span the Os(2)–Os(3) edge of the Os_3 unit via N(1) and C(11) atoms to afford a four-membered ring containing Os(2), Os(3), C(11) and N(1). The four-membered osmacycle is at 77.9 and 78.8° to the Os_3 plane in **3** and **4**, respectively. The pyridyl ring is planar with a mean deviation from the plane of 0.01 Å for **3** and 0.003 Å for **4**. The dihedral angle between the pyridyl plane and the four-membered ring, which share a common edge N(1)–C(11) is, respectively, 2.0 and 4.7° for **3** and **4**. A hydride ligand, located by potential-energy calculations [16], is also found to bridge the edge Os(2)–Os(3) in **3** and **4**. The dibridged metal–metal bonds Os(2)–Os(3) is the longest of the three (2.919(1) **3**, 2.927(1) Å **4**). The other two non-bridged Os–Os bonds in each structure are normal at 2.866(2) and 2.878(2) Å for **3** and 2.882(1) and 2.869(1) Å for **4**. The N=N bond distances (1.28(4) **3**, 1.24(4) Å **4**) indicate a significant amount of double bond character. There are no unusual structural or bonding features in the organic moieties of the cluster complexes. In terms of electron counting, each cluster is electron precise with 48 cluster valence electrons, provided that the 2-pyridyl ligand is regarded as a three-electron donor.

Table 6
Selected bond lengths (Å) and angles (°) for complex **3**

Bond lengths			
Os(1)–Os(2)	2.866(2)	Os(1)–Os(3)	2.878(2)
Os(2)–Os(3)	2.919(1)	Os(2)–N(1)	2.13(2)
Os(3)–C(11)	2.10(2)	N(1)–C(11)	1.36(3)
C(13)–N(2)	1.42(4)	N(2)–N(3)	1.28(4)
N(3)–C(16)	1.56(3)		
Bond angles			
Os(2)–Os(1)–Os(3)	61.07(4)	Os(1)–Os(2)–Os(3)	59.66(4)
Os(1)–Os(3)–Os(2)	59.27(4)	Os(2)–Os(3)–C(11)	68.0(7)
Os(3)–Os(2)–N(1)	68.8(6)	Os(2)–N(1)–C(11)	109(1)
Os(3)–C(11)–N(1)	113(1)	C(13)–N(2)–N(3)	106(3)
N(2)–N(3)–C(16)	113(3)		

Table 7
Selected bond lengths (Å) and angles (°) for complex **4**

Bond lengths			
Os(1)–Os(2)	2.882(1)	Os(1)–Os(3)	2.869(1)
Os(2)–Os(3)	2.927(1)	Os(2)–C(11)	2.12(2)
Os(3)–N(1)	2.13(2)	N(1)–C(11)	1.36(3)
C(13)–N(2)	1.46(3)	N(2)–N(2*)	1.24(4)
Bond angles			
Os(2)–Os(1)–Os(3)	61.18(3)	Os(1)–Os(2)–Os(3)	59.18(3)
Os(1)–Os(3)–Os(2)	59.64(3)	Os(2)–Os(3)–N(1)	68.0(5)
Os(3)–Os(2)–C(11)	68.5(6)	Os(2)–C(11)–N(1)	111(1)
Os(3)–N(1)–C(11)	111(1)	C(13)–N(2)–N(2*)	114(2)

3. Conclusions

A series of carbonyl complexes of tungsten and osmium containing the pyridyl-azo entity have been synthesized and structurally characterized by X-ray crystallography. Specifically, the successful isolation of two dimeric metal complexes bridged by 4,4′-azopyridine appears to be appealing in that they may serve as models for the study of metal–metal interactions. Although the ligand $\mathbf{L_2}$ has four possible sites of coordination, namely, the two pyridine nitrogens and the two azo nitrogens, our present work has shown that the azo (–N=N–) moiety does not contribute to the coordination properties of this ligand and no N=N bond cleavage was observed. It is also apparent that the tungsten pyridyl-azo complexes display strong negative solvatochromism and may provide additional information for the study of solvent effects on MLCT bands in transition metal complexes.

4. Experimental

4.1. General procedures

None of the compounds reported is particularly air-sensitive, but all manipulations were carried out under an atmosphere of dry dinitrogen using Schlenk techniques. Solvents were predried and distilled from appropriate drying agents [17]. All chemicals, except where stated, were purchased from commercial sources and used as received. The compounds $[Os_3(CO)_{10}(NCMe)_2]$ [18], 4-phenylazopyridine [19] and 4,4′-azopyridine [6] were prepared by literature methods. IR spectra were recorded as CH_2Cl_2 solutions on a Perkin–Elmer Paragon 1000 PC or Nicolet Magna 550 Series II IR spectrometer. The ^{1}H-NMR spectra were recorded on a Jeol EX270 FT-NMR spectrometer using deuteriated solvents as lock and the residual protons in the solvent as references. Chemical shifts are reported downfield positive relative to $SiMe_4$. Mass spectra were

Table 8
Crystal data and data collection parameters for complexes **1**–**4**

	1	**2**	**3**	**4**
Empirical formula	$C_{16}H_9N_3O_5W$	$C_{20}H_8N_4O_{10}W_2$	$C_{21}H_9N_3O_{10}Os_3$	$C_{30}H_8N_4O_{20}Os_6$
Formula weight	507.11	832.00	1033.92	1885.61
Crystal size (mm)	$0.32\times0.22\times0.14$	$0.31\times0.13\times0.12$	$0.18\times0.17\times0.12$	$0.21\times0.15\times0.14$
Crystal system	Triclinic	Monoclinic	Monoclinic	Monoclinic
Space group	$P\bar{1}$	$P2_1/n$	$P2_1/a$	$C2/c$
a (Å)	9.057(1)	6.189(3)	17.128(2)	38.119(4)
b (Å)	12.567(2)	15.448(2)	7.620(2)	7.657(3)
c (Å)	7.9934(8)	12.984(2)	21.396(2)	17.325(4)
α (°)	93.17(1)	90	90	90
β (°)	94.44(1)	102.46(2)	94.68(1)	99.69(1)
γ (°)	69.67(1)	90	90	90
U (Å^3)	850.2(2)	1212.2(5)	2783.3(6)	4984(1)
$D_{calc.}$ (g cm^{-3})	1.981	2.279	2.467	2.512
Absorption coefficient (cm^{-1})	68.32	95.54	137.07	152.91
Z	2	2	4	4
$F(000)$	480	768	1856	3328
$2\theta_{max}$ (°)	50.0	50.0	45.0	45.0
Scan type	$\omega-2\theta$	$\omega-2\theta$	$\omega-2\theta$	$\omega-2\theta$
Scan rate (° min^{-1} in ω)	16.0	16.0	16.0	16.0
Scan range (ω) (°)	$1.15+0.35\tan\theta$	$1.00+0.35\tan\theta$	$1.84+0.35\tan\theta$	$0.73+0.35\tan\theta$
Reflections collected	3198	2453	4127	3625
Independent reflections (R_{int})	2991 (0.030)	2238 (0.029)	3973 (0.028)	3559 (0.043)
Observed reflections [$I>n\sigma(I)$]	2404 ($n=1.5$)	1565 ($n=3.0$)	2342 ($n=3.0$)	2120 ($n=3.0$)
No. of parameters	208	163	280	136
Weighting scheme $w=[\sigma_c^2(F_o)+p^2/4F_o^2]^{-1}$	$p=0.020$	$p=0.026$	$p=0.021$	$p=0.012$
R, R_w	0.044, 0.048	0.056, 0.085	0.044, 0.059	0.039, 0.056
Goodness-of–fit	1.45	2.79	2.35	1.92
Residual extrema in final diff. map (e Å^{-3})	1.53 to −1.92 (close to W)	3.16 to −2.64 (close to W)	1.53 to −1.35 (close to Os)	1.59 to −1.09 (close to Os)

recorded on a Finnigan MAT 95 instrument by the FAB technique. Electronic absorption spectra were obtained with a Perkin–Elmer Lambda UV–vis spectrophotometer. Preparative TLC and column chromatography were performed in air on 1 mm Kieselgel 60 silica plates and Kieselgel 60 (230–400 mesh) silica gel, respectively.

4.2. Complex preparations

4.2.1. Synthesis of $[W(CO)_5(NC_5H_4–N=N–C_6H_5)]$ (1)

$W(CO)_6$ (0.10 g, 0.28 mmol) was suspended in dry THF (40 cm^3) in a flask fitted with a condenser jacket. The mixture was then irradiated with a 125 W medium-pressure mercury lamp whilst being stirred for about 1 h, until a golden-yellow solution corresponding to $[W(CO)_5(THF)]$ was obtained. The reaction progress was monitored by ν_{CO} IR spectroscopy. The solution mixture was filtered through a pad of Celite with a sintered glass funnel and one equivalent of the ligand $\mathbf{L_1}$ (0.051 g, 0.28 mmol) was subsequently added. The solution rapidly turned red. After stirring for 2 h, the solvent was evaporated under vacuum, and the residue chromatographed over silica using 4:1 hexane–CH_2Cl_2 (v/v) as eluent ($R_f=0.56$) to afford a major red band that was characterized as the desired product **1** (47%, 0.067 g). Found: C, 37.76; H, 1.70; N, 7.97. $C_{16}H_9N_3O_5W$ requires C, 37.90; H, 1.79; N, 8.29%.

4.2.2. Synthesis of $[(CO)_5W(\mu\text{-}NC_5H_4–N=N–C_5H_4N)W(CO)_5]$ (2)

The compound $[W(CO)_5(THF)]$ was prepared using the conditions described above for **1**. A half equivalent of the ligand $\mathbf{L_2}$ (0.026 g, 0.14 mmol) was then added to the yellow solution, which became dark purple. The solution was stirred for about 2 h after which time the solution was evaporated to dryness in vacuo. The product was purified by column chromatography on silica with 1:1 hexane–CH_2Cl_2 (v/v) as eluent. The major purple band ($R_f=0.60$) was collected and the solution was evaporated to dryness to give a deep-purple powder in 53% yield (0.12 g). Found: C, 28.58; H, 1.02; N, 6.55. $C_{20}H_8N_4O_{10}W_2$ requires C, 28.87; H, 0.97; N, 6.73%.

4.2.3. Synthesis of $[Os_3(\mu\text{-}H)(CO)_{10}(\mu\text{-}NC_5H_3–N=N–C_6H_5)]$ (3)

The activated cluster $[Os_3(CO)_{10}(NCMe)_2]$ (50 mg, 0.054 mmol) and the ligand $\mathbf{L_1}$ (10 mg, 0.054 mmol) in CH_2Cl_2 (25 cm^3) were stirred for 2 h at room tempera-

ture. At the end of the reaction the color of the mixture changed from yellow to orange. Then, the volume was reduced to 3 cm^3. Purification was accomplished by preparative TLC using 9:1 hexane–CH_2Cl_2 (v/v) as eluent to afford complex **3** ($R_f = 0.45$), which was recrystallized from hexane–CH_2Cl_2 to afford an orange crystalline solid in 41% (23 mg) yield. Found: C, 24.28; H, 0.84; N, 3.96. $C_{21}H_9N_3O_{10}Os_3$ requires C, 24.40; H, 0.88; N, 4.06%.

*4.2.4. Synthesis of $[Os_3(\mu\text{-}H)(CO)_{10}(\mu\text{-}NC_5H_3\text{–}N{=}N\text{–}C_5H_3N)Os_3(\mu\text{-}H)(CO)_{10}]$ (**4**)*

Two molar equivalents of $[Os_3(CO)_{10}(NCMe)_2]$ (50 mg, 0.054 mmol) and the corresponding ligand $\mathbf{L_2}$ (5 mg, 0.027 mmol) were mixed and dissolved in CH_2Cl_2 (25 cm^3). The solution was stirred at room temperature and immediately turned red. After stirring for 1 h, the resulting mixture was concentrated to about 3 cm^3. Subsequent TLC separation eluting with 7:3 hexane–CH_2Cl_2 (v/v) gave a major deep-red band ($R_f = 0.65$), which was isolated and identified as the desired dimeric product **4** after recrystallization from CH_2Cl_2 (yield 52%, 26 mg). Found: C, 19.05; H, 0.31; N, 2.90. $C_{30}H_8N_4O_{20}Os_6$ requires C, 19.11; H, 0.43; N, 2.97%.

5. Crystallography

Single crystals suitable for X-ray crystallographic analyses for all compounds in this study were chosen and mounted on a glass fiber using epoxy resin. Diffraction data were collected at room temperature on a Rigaku AFC7R diffractometer using graphite-monochromated Mo–K_α radiation ($\lambda = 0.71073$ Å) and $\omega - 2\theta$ scan technique. Unit-cell parameters were determined from 25 accurately centered reflections. The stability of crystals were monitored at regular intervals using three standard reflections and no significant decay was observed. The intensity data were corrected for Lorentz and polarization effects. Absorption corrections by the ψ-scan method were applied. Space groups for all crystals were determined from a combination of Laue symmetry check and their systematic absences, which were then confirmed by successful refinement of the structures. All the structures were solved by direct methods (SHELXS-86 [20] for **1**, SIR92 [21] for **2**–**4**), and expanded by difference Fourier techniques. Structure refinements were made on F by full-matrix least-squares analysis. For **1**, the nitrogen atoms N(2) and N(3) of the azo group showed positional disorder and they were modeled with a two-site model with occupancy factors of 0.5 each but were not refined. Attempts to refine these parameters led to a chemically unreasonable model. All other non-hydrogen atoms were assigned with anisotropic displacement parameters. For **2**, all non-hydrogen atoms were refined anisotropically. Initial attempts to isotropically refine the carbon atoms (C(16) to C(21)) of the phenyl ring in **3** led to unreasonably high B_{eq} values. These atoms were then fixed throughout in the subsequent refinement cycles. For **4**, only Os atoms were assigned with anisotropic displacement parameters. The hydrogen atoms of the organic moieties were generated in their idealized positions whereas all metal hydrides were estimated by potential energy calculations [16]. All calculations were performed on a Silicon-Graphics computer using the program package TEXSAN [22].

6. Supplementary material

Crystallographic data (comprising hydrogen atom coordinates, displacement parameters and full tables of bond lengths and angles) for the structural analysis have been deposited with the Cambridge Crystallographic Center (deposition nos. CCDC 133377–133380). Copies of this information may be obtained free of charge from The Director, CCDC, 12 Union Road, Cambridge, CB2 1EZ, UK (Fax: +44-1223-336033; e-mail: deposit@ccdc.cam.ac.uk or www: http://www.ccdc.cam.ac.uk).

Acknowledgements

We acknowledge The Hong Kong Baptist University (W.-Y.W.) for financial support.

References

[1] F.A. Cotton, G. Wilkinson, C.A. Murillo, M. Bochmann, Advanced Inorganic Chemistry, sixth ed., Wiley, Chichester, 1999.
[2] E.E. Bunel, L. Valle, N.L. Jones, P.J. Carroll, M. Gonzalez, N. Munoz, J.M. Manriquez, Organometallics 7 (1988) 789.
[3] J.T. Lin, S.-S. Sun, J.J. Wu, L. Lee, K.-J. Lin, Y.F. Huang, Inorg. Chem. 34 (1995) 2323.
[4] G.L. Geoffroy, M.S. Wrighton (Eds.), Organometallic Photochemistry, Academic Press, New York, 1979.
[5] (a) D.R. Kanis, M.A. Ratner, T.J. Marks, Chem. Rev. 94 (1994) 195. (b) M. Bourgault, W. Tam, D.F. Eaton, Organometallics 9 (1990) 2856.
[6] J.-P. Launay, M. Tourrel-Pagis, J.-F. Lipskier, V. Marvaud, C. Joachim, Inorg. Chem. 30 (1991) 1033.
[7] V.W.W. Yam, V.C.Y. Lau, L.-X. Wu, J. Chem. Soc. Dalton Trans. (1998) 1461.
[8] See for example: (a) M. Tasi, A.K. Powell, H. Vahrenkamp, Chem. Ber. 124 (1991) 1549. (b) H. Bantel, B. Hansert, A.K. Powell, M. Tasi, H. Vahrenkamp, Angew. Chem. Int. Ed. Engl. 28 (1989) 1509. (c) J.A. Smieja, J.E. Gozum, W.L. Gladfelter, Organometallics 6 (1987) 1311. (d) B. Hansert, H. Vahrenkamp, Chem. Ber. 126 (1993) 2017; 2023. (e) W.-T. Wong, T.-S. Wong, J. Organomet. Chem. 542 (1997) 29.
[9] Y.-K. Au, K.-K. Cheung, W.-T. Wong, Inorg. Chim. Acta 238 (1995) 193.

[10] (a) M.M. Zulu, A.J. Lees, Inorg. Chem. 27 (1988) 1139. (b) C.S. Kraihanzel, F.A. Cotton, Inorg. Chem. 2 (1963) 533.
[11] (a) C.C. Yin, A.J. Deeming, J. Chem. Soc. Dalton Trans. (1975) 2091. (b) A.J. Deeming, R. Peters, M.B. Hursthouse, J.D.J. Backer-Dirks, J. Chem. Soc. Dalton Trans. (1982) 787. (c) W.-Y. Wong, W.-T. Wong, J. Chem. Soc. Dalton Trans. (1996) 1853; 3209.
[12] A.J. Arce, C. Acuña, A.J. Deeming, J. Organomet. Chem. 356 (1988) C47.
[13] S. Sakanishi, D.A. Bardwell, S. Couchman, J.C. Jeffery, J.A. McCleverty, M.D. Ward, J. Organomet. Chem. 528 (1997) 35.
[14] (a) D.M. Manuta, A.J. Lees, Inorg. Chem. 25 (1986) 3212. (b) B.P. Sullivan, J. Phys. Chem. 93 (1989) 24. (c) R.N. Dominey, B. Hauser, J. Hubbard, J. Dunham, Inorg. Chem. 30 (1991) 4754.
[15] (a) J.T. Lin, P.S. Huang, T.Y.R. Tsai, C.Y. Liao, L.H. Tseng, Y.S. Wen, F.K. Shi, Inorg. Chem. 31 (1992) 4444. (b) D. Osella, L. Milone, C. Nervi, M. Ravera, J. Organomet. Chem. 488 (1995) 1.
[16] A.G. Orpen, J. Chem. Soc. Dalton Trans. (1980) 2509.
[17] W.L.F. Armarego, D.D. Perrin, Purification of Laboratory Chemicals, fourth ed., Butterworth–Heinemann, Guildford, UK, 1996.
[18] J.N. Nicholls, M.D. Vargas, Inorg. Synth. 28 (1990) 289.
[19] N. Campbell, A.W. Henderson, D. Taylor, J. Chem. Soc. (1953) 1281.
[20] G.M. Sheldrick, in: G.M. Sheldrick, C. Kruger, R. Goddard (Eds.), Crystallographic Computing, third ed., Oxford University Press, Oxford, UK, 1985, pp. 175–189.
[21] A. Altomare, M.C. Burla, M. Camalli, M. Cascarano, C. Giacovazzo, A. Guagliardi, G. Polidori, J. Appl. Crystallogr. 27 (1994) 435.
[22] TEXSAN, Crystal Structure Analysis Package, Molecular Structure Corporation, Houston, TX, 1985 and 1992.